POLITECNICO
MILANO 1863

SCUOLA DI INGEGNERIA INDUSTRIALE
E DELL'INFORMAZIONE

Executive Summary of the Thesis

X-Ray Raman characterization of CO conversion to CO_2 on Au/CeO_2 substrate

Laurea Magistrale in Engineering Physics

Author: Eugenio Bianchi

Advisor: Prof. Marco Moretti

Co-advisor: Alessandro Longo, Christoph J. Sahle

Academic year: 2022-2023

Abstract

Technologies for the conversion and removal of hazardous gasses are becoming indispensable to the fight on climate change. Ceria with gold nanoparticles precipitated on the its surface has shown interesting properties for this topic, catalysing the conversion CO to CO_2 thanks to its oxygen storage capacity (OSC). The scope of this thesis is following the change in the Oxidation State (OS) of Ce ions, connected to the release/uptake of oxygen by the substrate, through the changes in the the spectral features of the Ce $N_{4,5}$ excitation edge, involving Ce $4d$ and $4f$ levels. This analysis led to the quantification of the ratio between Ce^{4+}/Ce^{3+}. *In situ* X-ray Raman Scattering (XRS) spectroscopy experiments, sensitive to the electronic configuration of the sample, have been conducted at the ID20 beamline at ESRF. The $N_{4,5}$ excitation edge has been scanned and the edge and pre-edge feature measured. Multiplet calculations have been performed with the Hilbert++ code to simulate the spectral features of the $N_{4,5}$ edge for Ce. Upon CO and temperature treatment, the conversion from Ce^{4+} to Ce^{3+} led to roughly 30% of Ce^{3+} concentration in the sample .

1. Introduction

The rapid climate change has lately focused a lot of attention on new mitigation and adaptation techniques to reduce and coexist with the damages caused by the current society fossil-fuels-based for energy production. Carbon capture and hazardous gasses conversion and removal will become indispensable. Because they act as catalysts and catalysts support in this field, Rare Earth Element (REE) based materials will play an important role in the fight against climate change. They have been proved to work as three way catalysts (TWCs) for CO conversion to CO_2 [5], removing this dangerous gas from the emissions of industries and vehicles.

Because of its unique high OSC, ceria, or CeO_2, remains one of the main REE oxides studied for these catalytic purposes. The activity of Au for CO conversion has been long long studied [3], Au on a ceria substrate facilitates the O vacancy formation process lowering the reaction temperature, enhancing the catalytic activity. Au nanoparticles (NPs) have shown promising O activation properties. The study of the reaction pathway led to a Mars-van Krevelen mechanism, shown in Figure 1. A lot of studies have been conducted to investigate the catalytic ac-

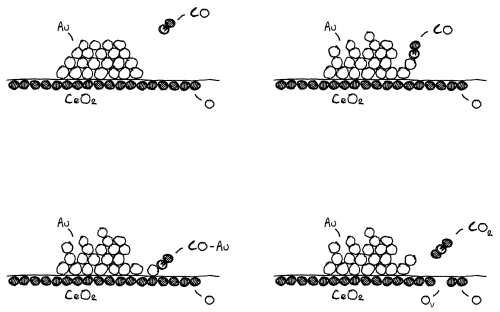

Figure 1: Dynamics of the redox process for small NPs. The CO molecule bounds to a Au ion on the NP surface. This Au-CO species moves from the NP surface to the Au/CeO_2 interface. Here the CO molecule oxidizes to CO_2 on the ceria surface removing one O ion and leaving a vacancy.

tivity of ceria. Atomic Force, Scanning Tunneling and Tunneling Electron Microscopy (AFM, STM and TEM respectively) methods have been used to follow the behavior of both ceria surface and Au NPs. To probe the amount of O vacancies, XRD and X-ray Absorption Near-Edge Spectroscopy (XANES) at the L_3 absorption edge of Ce experiments have been conducted; since O vacancy formation release two electrons that accommodate on the $4f$ orbital of two Ce ions, reducing them. In the energy range of this edge, the mixing of d and f Ce^{3+} orbitals complicates the analysis. All of the experimental methods discussed above, provide only a picture of the surface, and/or need difficult sample environment, like ultra high vacuum. In this thesis, a new method of following the reduction is proposed. X-ray Raman Scattering (XRS) spectroscopy experiments have been conducted *in situ* for the first time, at the $N_{4,5}$ edge of Ce, on ceria pellets with Au NPs precipitated on the surface. We gain direct knowledge on structure of $4f$ electrons as we look at the $4d$ to $4f$ transition. The samples underwent CO treatments at increasing temperatures, while XRS measurements were taken.

The goal of this thesis is the study of the oxidation process happening on a $1\%Au/CeO_2$ sample in anaerobic condition with temperature ranging from 25 to 600 °C, through this edge.

Ab initio DFT calculation and multiplet analysis have been performed with the Hilbert++ code to simulate the spectral features of the $N_{4,5}$ edge for Ce^{4+} and for Ce^{3+}. The results are used to infer on the Ce^{3+}/Ce^{4+} ratio correlated to the O vacancy concentration.

2. XRS foundations

Our many-body system can be described by an approximated Hamiltonian H_0 as:

$$H_0\Psi^0 = E^0\Psi^0. \tag{1}$$

The approximated many-body solutions to this equations are expressed with single electron wavefunctions ψ_k. The ψ_k can be expressed with a radial, an angular, and a spinor component: $\psi_k = R_{n,l}(\mathbf{r})Y_{l,m_l}(\theta,\phi)\ \chi_{m_s}$. The solutions to the many body Schrödinger equation (1) have to be fully anti-symmetric and can be expressed through a Slater determinant. In the XRS experiment conducted, an x-ray beam impinges on the sample. The interaction between the electromagnetic field of the incident x-ray beam and a charged particle is described by the following Hamiltonian:

$$H_{int} = \sum_j \frac{e^2}{2mc^2}\boldsymbol{A}_j^2 + \sum_j \frac{e}{mc}\boldsymbol{p}_j\cdot\boldsymbol{A}_j, \tag{2}$$

$\boldsymbol{p}_j$ and $\boldsymbol{A}_j$ are the momentum of the j-th electron and the vector potential of the electromagnetic field [4]. For the experiment presented in this thesis only the first term will be of interest. The interaction Hamiltonian can therefore be divided in to terms, $H_{int} = H_{i1} + H_{i2}$. With $H_{i1} = \sum_j \frac{e^2}{2mc^2}\boldsymbol{A}_j^2$, and using the *Fermi Golden Rule*, we can derive the following XRS double differential scattering cross section

$$\frac{d^2\sigma}{d\Omega_2 d\omega_2} \propto \frac{2\pi}{\hbar}|\langle f|H_{i1}|i\rangle|^2\delta_{\Delta E_{f,i}-\hbar\omega}$$

$$\frac{d^2\sigma}{d\Omega_2 d\omega_2} = \left(\frac{d\sigma}{d\Omega_2}\right)_{Th} S(\boldsymbol{k},\omega),$$

with $(d\sigma/d\Omega_2)_{Th} = r_0^2(\omega_2/\omega_1)(\boldsymbol{e}_1\cdot\boldsymbol{e}_2)^2$ which is the Thomson scattering differential cross section, and

$$S(\boldsymbol{k},\omega) = \sum_f |\langle f|\sum_j e^{-i\boldsymbol{k}\cdot\boldsymbol{r}_j}|i\rangle|^2\delta_{\Delta E_{f,i}-\hbar\omega} \tag{3}$$

is the dynamic structure factor. The $\Delta E_{f,i}$ is the difference between the energy of the final

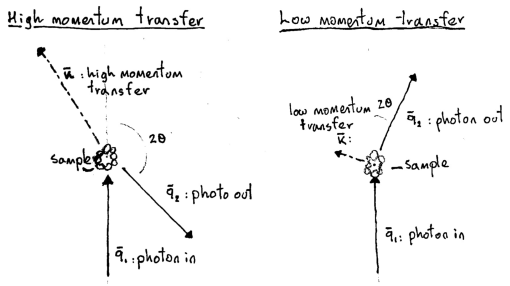

Figure 2: Schematics of the XRS process. The incoming and scattered photons have a wavevector $\boldsymbol{k}$ and $\boldsymbol{k'}$, the momentum transfer $\boldsymbol{q}_{l,h}$ is equal to $\boldsymbol{k'} - \boldsymbol{k}$

and the initial state. This cross section describes the interaction shown in Figure 2. For low $\boldsymbol{k}$ the exponential term in the dynamic structure factor can be expanded as:

$$e^{-i\boldsymbol{k}\cdot\boldsymbol{r}_j} \approx 1 + i\boldsymbol{k}\cdot\boldsymbol{r}_j - (\boldsymbol{k}\cdot\boldsymbol{r}_j)^2/2 + \dots. \quad (4)$$

When $\boldsymbol{k}\cdot\boldsymbol{r}_j \ll 1$, replacing (4) in (3), we obtain a term proportional to $\langle f|1|i\rangle = 0$, and a dipolar term proportional to $\langle f|i\boldsymbol{k}\cdot\boldsymbol{r}_j|i\rangle$, that dominates over the subsequent terms. This term has the same dependence on the wavevector $\boldsymbol{k}$ and on the electrons position $\boldsymbol{r}_j$ of an absorption cross section, described by the second term on the right hand side of (2), the same that describe the transition in XAS experiments, where a photon with wave vector $\boldsymbol{k}$ is completely absorbed by the system. Increasing the momentum transfer the Taylor expansion breaks down and terms others than the first dipolar one become dominant. In this case it is more convenient to expand the vector potential in spherical harmonics

$$e^{-i\boldsymbol{k}\cdot\boldsymbol{r}} = \sum_{q=0}^{+\infty}\sum_{m=-q}^{q} i^q(2q+1)j_q\cdot C^*_{q,m}\cdot C_{q,m},$$

here the j_q are spherical Bessel function of the q-th order, the $C_{q,m} = \sqrt{4\pi/(2q+1)}Y_{q,m}$ are the normalized spherical harmonics. The initial and final state of the system are written as the product of one-particle wavefunctions, which are themselves expressed as the product of a radial function R_j, and a spherical harmonic $Y_{q,m}$. The term inside the bra-ket of (3) can therefore be written as:

$$\langle f|e^{-i\boldsymbol{k}\cdot\boldsymbol{r}}|i\rangle = \sum_{q,m} A_{q,m}I_{q,m}$$

with $A_{q,m} = i^k(2q+1)C^*_{q,m}\langle R_f|j_q|R_i\rangle$, and $I_{q,m} = \langle Y_{l_f,m_f}|C_{q,m}|Y_{l_i,m_i}\rangle$. The radial matrix element, links the probability of a transition from $|i\rangle$ to a certain $|f\rangle$, with the the Bessel function j_q; it has a different maximum for different orders q; at higher momentum transfer, the contribution to the spectrum will be given by higher order transition. This matrix element is at its highest when the two radial function have the same principal quantum number. For this reason it is better to look at the $N_{4,5}$ edge, involving $4d$ and $4f$ states, than the $M_{4,5}$, which involve the $3d$ to $4f$ transitions. The angular matrix element sets the selection rules of the transition. Through x-ray Raman scattering it is possible to chose the momentum transfer of the transition and access also the transition over the dipole that would prohibited by normal XAS. During the experiment performed for this thesis, the transition at the $N_{4,5}$ edge of Ce^{4+} and Ce^{3+} are probed. The initial electronic configuration are [Xe]$4f^0$ and [Xe]$4f^1$, respectively. This edge of x-ray absorption involves the transition of $4d$ electrons into the $4f$ shell. Through x-ray Raman scattering it is possible to chose the momentum transfer of the transition and access also the transition over the dipole that would prohibited by normal XAS, as the dipole term, responsible for the transition at low $\boldsymbol{q}$, gets less relevant than the other terms, thus allowing for out of dipole transition.

3. Experimental technique and setup

The experiments and the analysis reported were conducted at the ID20 at ESRF, the European Synchrotron Research Facility. ID20 is equipped with a large-solid-angle XRS spectrometer, used for the experiment reported here. The whole spectrometer consists in 6 mobile units, each one containing 12 spherically bent analyzer crystals and a 2D detector, shown in Figure 3. The analyzer crystals and the 2D detectors are located on a Rowland circle, working in a Johann configuration[1]. The data is collected by the 2D detectors mounted on the units. An image of the

[1]This means that the sample, the analyzer crystals and the detectors are all aligned on the surface of a virtual circle, called a Rowland circle. The light scattered from the sample hits the spherically bent crystals and is focused on the detectors.

Figure 3: Photo of the large-solid-angle x-ray Raman spectrometer, here are visible five of the six units independently movable.

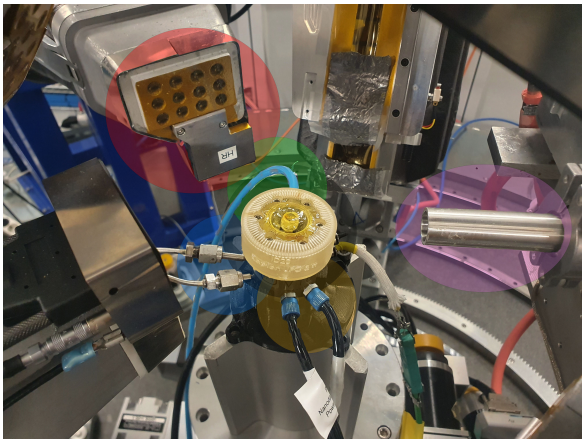

Figure 4: Sample environment at ID20 for XRS experiments. In the center of the picture is located the ceria sample used in the experiment, inside the air-tight dome. In the center black circle, it is located the ceria sample used in the experiment in the sample holder. Attached to the sample holder, in the orange circle, the two black cables control the furnace; the two silver cables in the blue circle, they are used to pump the 1%CO/He in and the reaction gas out; in the green circle, the blue cable is used to pump nitrogen for cooling. In the red circle, the yellow holed plate is the entrance for the scattered beam hitting the twelve analysing crystals in the HR unit. The silver shape attached underneath the HR unit, is the detector. In the purple ellipse, there is the metal tube from where the synchrotron beam comes and hits the sample.

sample is generated on the detector where the intensity of the scattered beam is measured. The signal from the same units are summed up and the XRS spectrum is obtained. The interest of the experiment was the excitation spectrum of the sample, so only in the difference between the frequency of the incoming photons and the scattered one, $\omega = \omega_1 - \omega_2$.
XRS scans have been performed in the energy loss range of 0 to 700 eV with a step size of 1 eV[2]; later the energy loss range between 95 and 150 eV has been probed with a step size of 0.2 eV. The overall resolution of 0.7 eV has been obtained. To collect the data presented in this thesis, only the 24 analysing crystals of the VD and VB units were used. These units have been positioned at angles allowing for a momentum transfer of 3.5 and 9.5 $\pm$ 0.4 $Å^{-1}$. The temperature has been changed during the collection, starting from 25 °C and reaching gradually by variable steps 600 °C. The sample was prepared starting from a pellet of ceria Sigma-Aldrich, as received. The concentration required was obtained through homogeneous deposition precipitation, using urea as precipitation agent. Various pellets were left in a solution containing Au, for 16 hours at 80 °C under stirring. Then the pellets were dried and cleaned with water until no more of the urea's chloride ions were detected, using an $AgNO_3$ test. Among the pellets the one with 1 wt% Au NPs was chosen and used for the experiment (1%Au/CeO_2).
For the reference spectra of Ce when it is in the two different OSs, Ce^{3+} and Ce^{4+}, two pellets of pure ceria aldrich and cerium(III) sulphate were used. The samples have been encapsulated in a chamber, made by the sample holder and a transparent air-tight dome, mounted on a furnace, and placed in the center of the spectrometer. A picture of the setup is shown in figure 4. The chamber was initially flushed with pure He at 20 ml/min. To reduce the Ce in the ceria pellets from Ce^{4+} to Ce^{3+}, a mixture of He/1%CO was fluxed in the chamber for 120 minutes. The expectation was that ceria would donate some of the O it stores to the gas oxidizing CO to CO_2. Afterwards the chamber has been fluxed with pure He for 30 minutes, and later a mixture of He/20%O_2 for 60 minutes. The data of the XRS experiment were collected *in situ*.

[2]Ce $N_{4,5}$ edge is located at lower energies, but together with this edge, also the O K edge has been probed, located between 520 and 590 eV.

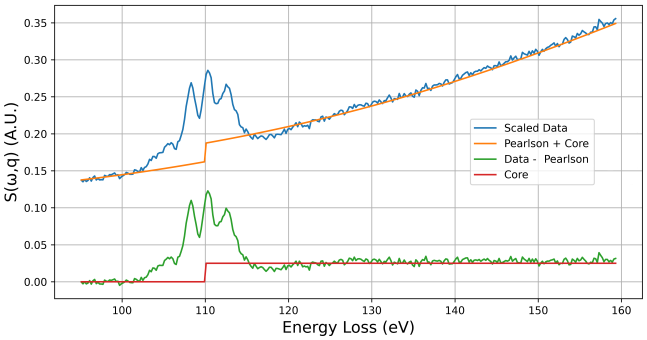

Figure 5: Spectra from the x-ray Raman scattering obtained at the $N_{4,5}$ of cerium(III) with a momentum scattering of $\boldsymbol{q} = 9.5$ Å^{-1}. The blue line is the spectra obtained from all twelve the analyzing crystals collected at the detector in the module VB. The green curve is the signal obtained after the removal of the Compton profile.

4. Data analysis and results

The scope of the experiment was following the reduction process of ceria pellets coated with Au NPs, to quantify the ratio between two different OSs of Ce, Ce^{4+}/Ce^{3+}, through the analysis of the changes in the XRS excitation spectra at the $N_{4,5}$ of Ce, whilst changing the temperature and the gas environment of the sample. At ID20 the Python library *XRStools* is implemented. This library allows for an easy extraction of the data and a preliminary analysis, an example is shown in Figure 5.

As shown in figure 6, the CO treatment changes the spectra of ceria as the temperature is increased. While the reduction of the sample Ce ions takes place, some electrons hop from $2p$ orbitals of the O ions to the Ce $4f$ orbitals. At low momentum transfer, just the dipole giant resonance is visible in the spectrum; some changes are noticeable while the CO treatment is going on. The shoulder at 125 eV becomes slightly more pronounced as the peak at 133 eV decreases. At high momentum transfer the spectra is dominated by the non-dipole transitions, highly sensitive to the treatment. The peaks at 112 eV and 108 eV decrease, and a peak at 110 eV appears between them, the small peak at 106 eV increases slightly and the spectrum broadens on the left end of the pre-edge features. To interpret the data, the Hilbert++ code was used to compute the multiplet spectra. With Hilbert++ it is possible to reproduce the q-dependence of XRS spectra with good agreement with the experiments. This code is able to take into account the environment effects of neighbouring ions to the absorbing one, and differently from similar codes that achieve the same good results, it does not require a specific symmetry group for the crystal. The spectra obtained with Hilbert++ have been shifted in energy to match the peaks position obtained experimentally, then they have been convoluted with a Fano resonance line shape functions to reproduce the broadening due to the life-time of the excited state, and the broadening due the experimental setup. The next step is to overlap the spectra obtained from the Au coated ceria sample at different temperature with a weighted sum of the two reference spectra $S_{calc} = w_{Ce^{3+}}\, S_{calc,Ce^{3+}} + w_{Ce^{4+}}\, S_{calc,Ce^{4+}}$. The simulations and the analysis reproduce well the experimental results. As explained in the literature [2], Ce in the OS Ce^{3+} has an electronic configuration of $[Xe]4f^1$, and presents two peaks at the $N_{4,5}$ edge for the giant dipole, one at 120 eV and one at 125 eV. Calculation performed for Ce^{4+}, in configuration $[Xe]4f^0$, should present just one peak at the same edge. It is observed

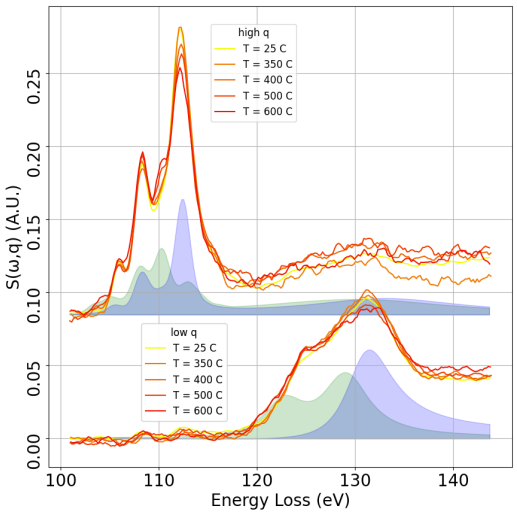

Figure 6: This are the experimental spectra obtained after the analysis. The green and purple shaded area below the curve are the simulated spectra for Ce^{3+} and Ce^{4+} respectively. It is evident that increasing the temperature from 25 °C to 600 °C, the spectral features change showing a contribution coming from Ce^{3+} more and more important.

that at the beginning of the CO treatment at room temperature, 1%Au/CeO_2 presents two peaks, one at 124 eV and one at 133 eV, indicating that already at low temperature there is a Ce^{3+} component in the ceria sample.
It was then possible to quantify how much Ce^{3+} is present in the sample at the end of the treatment. Using the reference computed spectra for Ce^{3+} and Ce^{4+}, a weighted sum of the two references have been done, where the weights represent the fraction of each species present in the sample. The weights have been chosen to match the computed spectrum with the experimental spectrum. We obtained that at low temperature, 1%Au/CeO_2 has already a Ce^{3+} component of 15%, after the CO treatment, at 600 °C, the the amount of Ce^{3+} increases up to 30∼35% of the total.

5. Conclusions

For the first time *in-situ* XRS measurements at the Ce $N_{4,5}$ edge have been performed to follow the reduction of Ce^{4+} to Ce^{3+}. This method can be used to study the O vacancy formation and concentration on ceria based materials and deepens the knowledge on the electronic properties of this REE oxide. We have shown how the analysis conducted on the excitation spectra at the $N_{4,5}$ edges and pre-edges of Ce can be effectively used to quantify the ratio of Ce^{3+}/Ce^{4+} in the ceria sample. It is worth noting that the high momentum transfer spectra show much clearer changes. The narrower peaks at high $\boldsymbol{q}$ are due to the fact these peaks are less affected by the interaction of the electrons with the continuum, which instead broadens the spectral features. The ceria sample covered with Au NPs shows good catalytic properties for the the oxidation of CO into CO_2.In particular, the Au ability to adsorb the CO molecules at higher temperature and lower partial pressure of the gas allows to obtain a conversion at lower temperatures with respect to pure ceria. The effect of hybridization on the spectra has not been previously discussed for the $N_{4,5}$ edge. It emerged especially from the low momentum transfer spectra that a model taking into consideration a partial hybridization of the O and cerium(IV) ions atomic orbitals is needed [1]. Taking into consideration the simulated spectra where we included some hybridization, it was found that a good match of the experimental data is obtained with 10% of Ce^{3+} at room temperature, which is slightly less that the 15% estimate done without the hybridization, and 30% at 600 °C

Acknowledgements

I want to thanks in particular Alessandro Longo and Christoph J. Sahle for having guided me throughout my experience at ESRF and well beyond, teaching me stuff, showing me other and suggesting the rest, and also for reviewing my thesis; Prof. Marco Moretti for the same, all giving me the opportunity to conduct my thesis at the ESRF. Thanks to Emmanuelle de Clermont Gallerande for having conducted the experiments with us (with us mainly in her way), to Blanka Detlefs, Florent Gerbon, and Quentin Faure for the support they gave me at ID20, to Alessandro Mirone for taking the time to explain me his code and providing the templates to use it.

References

[1] Tomá š Duchoň, Marie Aulická, Eike F. Schwier, Hideaki Iwasawa, Chuanlin Zhao, Ye Xu, Kate řina Veltruská, Kenya Shimada, and Vladimír Matolín. Covalent versus localized nature of $4f$ electrons in ceria: Resonant angle-resolved photoemission spectroscopy and density functional theory. *Phys. Rev. B*, 95:165124, Apr 2017.

[2] R. A. Gordon, G. T. Seidler, T. T. Fister, M. W. Haverkort, G. A. Sawatzky, A. Tanaka, and T. K. Sham. High multipole transitions in nixs: Valence and hybridization in 4f systems. *Europhysics Letters*, 81(2):26004, dec 2007.

[3] Masatake Haruta, Tetsuhiko Kobayashi, Hiroshi Sano, and Nobumasa Yamada. Novel gold catalysts for the oxidation of carbon monoxide at a temperature far below 0 °c. *Chemistry Letters*, 16(2):405–408, 1987.

[4] K Hämäläinen and S Manninen. Resonant and non-resonant inelastic x-ray scattering. *Journal of Physics: Condensed Matter*, 13(34):7539, aug 2001.

[5] M. Ozawa and C.-K. Loong. In situ x-ray and neutron powder diffraction studies of re-

dox behavior in ceo2-containing oxide catalysts. *Catalysis Today*, 50(2):329–342, 1999.